

KATARZYNA KOZIEŁ ^{1*}, NORBERT SKOCZYŁAS ²**ROCK TRANSPORT AFTER AN OUTBURST AND THE FLUIDISATION PHENOMENON
– CAN IT OCCUR DURING A DOLOMITE AND GAS OUTBURST?**

Rock and gas outburst is a phenomenon in which fragmented rock material is transported deep into a pit. The transport of rock material by gas is a two-phase process. The article deals with the fluidisation of rock material. Considerations on the fluidisation phenomenon were carried out, and experiments were performed to help clarify whether the fluidisation of dolomite is possible. In the last chapter, a discussion was carried out, and the results obtained were analysed regarding the possibility of occurrence in mine conditions.

Keywords: Rock and gas outburst; fluidisation; transport of post-outburst masses; gas energy; dolomite

1. Introduction

The exploitation of underground deposits is related to the occurrence of natural hazards such as those resulting from excavation depth, tectonic disorders, water flowing into mining excavations or the presence of gas located above the deposit space [1-6]. For decades, scientists across the world have studied all the adverse phenomena that have occurred to identify them and develop numerous theories, devices or forecasting methods, as well as their prevention [7-18].

Among all the risks, those related to the presence of gas in crevices or in the porous structure of the deposit seem to be the most important. These include high concentrations of gases harmful to health, methane explosions, and rock and gas outbursts etc. The problem of gas-geodynamic phenomena has been a current topic in coal mining for 150 years [19-22]. Gas-geodynamic phenomena

¹ STRATA MECHANICS RESEARCH INSTITUTE OF THE POLISH ACADEMY OF SCIENCE, 27 REYMONTA STR., 30-059 KRAKÓW, POLAND

² AGH UNIVERSITY OF KRAKOW, AL. MICKIEWICZA 30, 30-059 KRAKOW, POLAND

* Corresponding author: koziel@imgpan.pl



© 2023. The Author(s). This is an open-access article distributed under the terms of the Creative Commons Attribution-NonCommercial License (CC BY-NC 4.0, <https://creativecommons.org/licenses/by-nc/4.0/deed.en>) which permits the use, redistribution of the material in any medium or format, transforming and building upon the material, provided that the article is properly cited, the use is non-commercial, and no modifications or adaptations are made.

are rare, except for in rich copper deposits embedded in dolomite rocks [23-27], as well as in other hard rocks. In 2009, the first outburst of dolomite and gas took place [28-31], which resulted in the formation of a ca. 250 m³ cavern, while the transported, crushed rock material was strewn along 70 m of the heading. Subsequent events on such a large scale were recorded in 2015 when some 167 m³ of material was crushed, and in 2018, which resulted in the formation of a 219 m³ cavern, with the material being transported along approximately 30 m of the heading. In addition to these events, dozens of moderate gas-geodynamic events have been recorded over more than a decade.

The causes of rock and gas outbursts are listed as high rock porosity, increased sorption capacity of low gas permeability etc. [32-34]. Gas is stored in a well-developed porous structure of the rock with low permeability. The potential energy of the gas is released during an outburst event, and the amount of this energy strongly depends on the course of the sudden decompression [35,36]. The released energy is absorbed by rock crushing [18] and transported down the heading [37,38]. If coal and CH₄ or coal and CO₂ are ejected, the crushed coal undergoes intense desorption of the gas bound by sorption. This is related to the quadratic relationship between the intensity of gas emission from coal grains and their size and grain distribution of post-outburst masses, dominated by low fractions. Many researchers believe that adsorbed gas is mainly responsible for coal material transfer during outbursts [39-44], and this transport is characterised by fluidised flow. Dolomite is a rock characterised by marginal sorption phenomena occurring in it, which means that the energy of free gas accumulated in pores and crevices in the rock has to ensure both crushing and transport of the material. After studies dedicated to dolomite crushing [18] and initial studies on the transport of rock material [4], the authors have presented in this paper the possibility of fluidisation occurring in crushed dolomite during outburst, without the participation of gas bound through sorption.

2. Fluidisation in gas-geodynamic phenomena

Considerations related to fluidal flow during gas-geodynamic phenomena comprise an attempt at a slightly different analysis of transport. The transport of rock material through the gas is a two-phase process. If the fluid (gas) reaches a certain velocity range, in which the deposit reaches a “quasi-fluid” state, we can call this phenomenon fluidisation. In the case of rock and gas outburst, this will result in gas fluidisation. Fig. 1 presents the classical diagram depicting pressure exerted on the deposit on the velocity of the liquid jet. The boundaries of the deposit nature change are outlined in blue. In the case of CO₂ or CH₄ and coal outburst, the absorbed gas is largely responsible for the transport of crushed grains. Adequate intensity of gas desorption from finely crushed coal grains leads to the fluidisation of outburst products [39]. In rocks such as dolomite or anhydrite, sorption is negligible, however, the adequate quantity of gas emitted from the porous volume of rocks crushed in an avalanche-like manner may guarantee such a transport velocity of individual grain classes that their minimum fluidisation velocity is exceeded, and thus, a fluidised bed is created from the specific grain class.

The first stage (1) of fluidisation, which corresponds to a typical flow of fluid through a stationary porous layer, can be attributed to the moment when larger rock fragments spill out of the cavern, and the outburst begins. This causes the material to fall to the bottom of the heading, gradually blocking its cross-section, resulting in an increase in the velocity of the gas continuously released from the porous volume of the rock during rock destruction, as well as an increase in pressure between the gas jet and the deposit closing the cross-section. The porosity of such

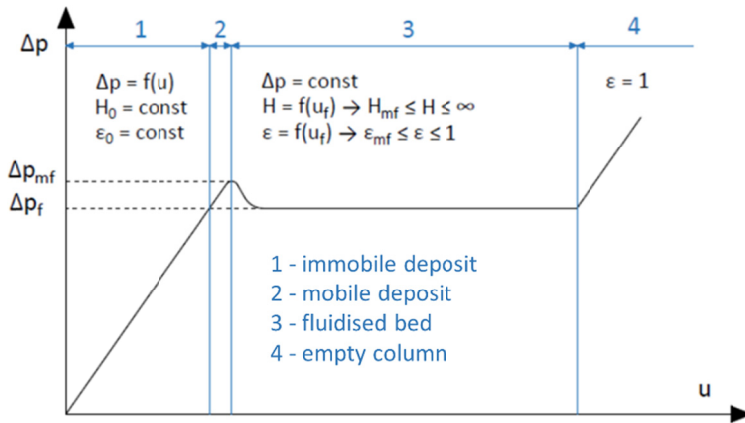


Fig. 1. Fluidised bed stages

a cast deposit depends on its bulk density. During stage (2), the immobile deposit is loosened, and this moment begins when the cross-section of the heading becomes partially opened during the outburst. Pressure reaches the maximum value and then gradually decreases. This is when stage (3) can begin for some grain classes if the minimum transport velocity is higher than the minimum fluidisation velocity. If the flow velocity becomes equal to the velocity of particle freefall, a boundary condition $\varepsilon = 1$ is created, at which fluidisation ends. If gas velocity continuously increased, the entire deposit would have been blown out (Stage 4).

The knowledge of individual fluidisation stages and the changes in physical parameters during each of the stages allows the stages to be defined using the appropriate mathematical equations. The authors assumed that the transport of the crushed rock is turbulent, thus the minimum fluidisation velocity for a turbulent flow may be described using equation (1) [45,46]:

$$u_{mf} = \sqrt{\frac{1}{1.75} \cdot \frac{g(\rho_s - \rho_G)d_s}{\rho_G} \cdot \varepsilon_{mf}^3} \quad (1)$$

where:

- u_{mf} – is the minimum fluidisation velocity, [m/s],
- g – is gravitational acceleration, [m/s²],
- ρ_s – is the skeleton density of the deposit, [kg/m³],
- ρ_G – is the gas density, [kg/m³],
- d_s – is the equivalent grain diameter, [m],
- ε_{mf} – the minimum porosity of the fluidised bed, [%].

If the minimum porosity of the fluidised bed is unknown, we need to use its approximation, which is usually in the range of $\varepsilon_{mf} = 0.35 \div 0.465$, then formula (2) defining the minimum fluidisation velocity becomes [46]:

$$u_{mf} = 0.2 \sqrt{\frac{g(\rho_s - \rho_G)d_s}{\rho_G}} \quad (2)$$

The equivalent grain diameter is included in the equations presented above. The grain classes of the rock material used in this paper were accepted according to the grain composition of post-outburst masses [4]. The equivalent grain diameter was determined according to equation (3), and the results are presented in TABLE 1:

$$d_s = \sqrt[3]{\frac{2 \cdot d_1^2 \cdot d_2^2}{d_1 + d_2}} \quad (3)$$

where:

d_1 – the diameter of the smallest grain in the considered grain class, [m],

d_2 – the diameter of the largest grain in the considered grain class, [m].

Knowledge of the density of gas-propelling deposit grains, deposit density and the equivalent diameter shall allow the determination of the minimum fluidisation velocity for individual grain classes. The average value of the range specified in the literature – $\varepsilon_{mf} = 0.408$ [46] was accepted as deposit porosity. The theoretical minimum fluidisation velocity is shown in TABLE 1.

TABLE 1

Determined equivalent diameter and theoretical, minimum fluidisation velocity

Grain class [mm]	Equivalent diameter [m]	Minimum fluidisation velocity [m/s]
20-50	0.0306	5.21
8-20	0.0122	3.30
4-8	0.0055	2.22
2-4	0.0028	1.57
1-2	0.0014	1.11

Once the bed reaches the maximum fluidisation velocity, its velocity continuously increases if a continuous gas supply is available, and fluidisation continues until the hovering velocity, equal to the freefall velocity of a particle in a static gas, is exceeded. Hovering velocity depends on the relationship between buoyancy forces and grain friction in the fluid and may be expressed using equation (4):

$$u_z = \frac{u_{mf}}{0.1175 - \frac{0.1046}{1 + 0.000373 Ar_f^{0.6}}} \quad (4)$$

where: Ar_f – the Archimedes number, [-].

The Archimedes number, used to describe the flow of particles and gas bubbles in fluids, is described by equation (5):

$$Ar_f = \frac{g \rho_G (\rho_s - \rho_G) d_s^3}{\eta_G^2} \quad (5)$$

where: η_G – dynamic viscosity of the fluid, [Pa · s].

The value of the Archimedes number characterises the motion type of a grain falling within the fluid. The value ranges for individual motion types are presented below:

- laminar range: $1.80 \cdot 10^{-3} < Ar_f < 7.20$,
- intermediate range: $7.20 < Ar_f < 3.30 \cdot 10^3$,
- turbulent range: $3.30 \cdot 10^3 < Ar_f < 8.25 \cdot 10^{10}$.

The Archimedes number and the theoretical hovering velocity were calculated for individual grain classes, assuming the dynamic viscosity of air at the level of $\eta_G = 1.72 \cdot 10^{-5}$ Pa·s and the provided equivalent grain diameter according to TABLE 1, and the results are presented in TABLE 2.

TABLE 2

The determined Archimedes number and the theoretical hovering velocity

Grain class [mm]	Archimedes number	Hovering velocity [m/s]
20-50	$3.18 \cdot 10^9$	44.55
8-20	$2.04 \cdot 10^8$	28.73
4-8	$1.90 \cdot 10^7$	20.80
2-4	$2.38 \cdot 10^6$	17.92
1-2	$2.97 \cdot 10^5$	19.62

The value of the Archimedes number determined according to the performed calculations indicates that the flow will be turbulent, which confirms the correct application of the equation for the minimum fluidisation velocity for turbulent flow. The obtained theoretical hovering speeds are in the range from 18 m/s to almost 29 m/s. The following chapter summarises these values, along with the results of the conducted experiments.

3. Experimental studies

Fluidisation is one of the types of two-phase transport, with one phase being continuous and the other – dispersed. In the case of coal outburst, a continuous supply of gas is provided thanks to desorption. Due to its marginal sorption capacity, in the case of dolomite, the well and uniformly developed, porous structure of the rock may be the source of gas supply, with the gas expanding from pores during crushing. A steady flow of gas allows the crushed material present in the deposit to be loosened, and fluidisation may occur if the appropriate velocity is maintained. An experiment intended to see whether a steady supply of gas to the deposit of dolomite grains is able to form a fluidised bed with such grains was performed to verify this hypothesis. Fig. 2a presents a diagram of the original measurement station used to perform the fluidisation experiments.

The measurement station included a fluidisation column, $D = 0.16$ m in diameter and $h = 2$ m tall, with a small, rigid sieve installed in the middle of the column, with the opening diameter of $d = 2 \cdot 10^{-4}$ m, intended to ensure uniform gas supply throughout the entire column diameter. This sieve contained rock material containing grain classes in percentages conforming to those present in post-outburst masses. The layer of rock material was poured up to the height of $h_s = 0.12$ m (Fig. 2b). The fluidisation column was connected to a fan, the speed of which was

adjusted using an inverter. A $D_p = 0.15$ m tube was installed in the suction part of the fan, where the velocity of the intake air was measured using a Pitot tube. This prepared station enabled the performance of the experiments.

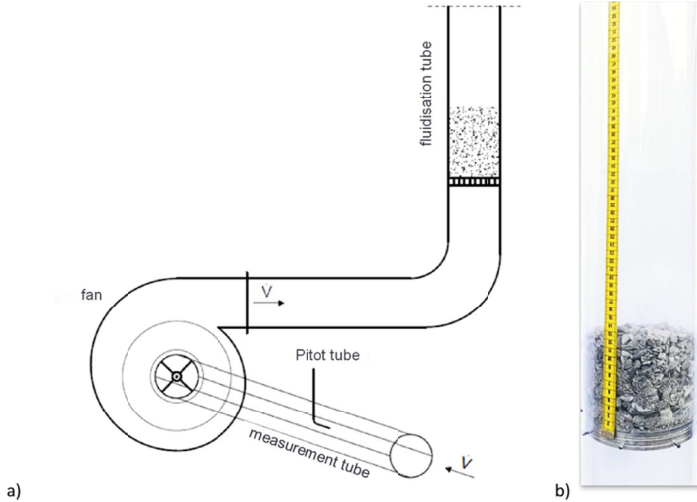


Fig. 2. The original measurement station for the fluidisation experiment

The experiment was started at the lowest achievable fan speeds, corresponding to the inverter frequency of 2 Hz, and those speeds were gradually increased by 2 Hz, approximately every 40 seconds, until the bed was started. The authors understand “bed starting” as a noticeable, minimal grain motion. The grains started to move only at the inverter frequency of 20 Hz, and thus, analyses were performed starting from this frequency. The experiment was a triplicate. Video documentation was recorded during the experiment in order to present the dynamic height of the material as a function of the pre-set airflow velocity.

The first of the main parameters required for the determination was the flow of intake air entering the measurement tube, which was expressed using formula (6):

$$\dot{V}_z = v_z \cdot \pi \left(\frac{D_p}{2} \right)^2 \quad (6)$$

where:

- \dot{V}_z – intake air-flow, [m³/s],
- v_z – intake air velocity, [m/s],
- D_p – measurement tube diameter, [m²].

Fig. 3 shows the recorded values of intake air velocity as a function of time (Fig. 3a), as a direct measurement result, as well as the averaged velocities as a function of the frequency pre-set at the fan inverter (Fig. 3b), which were used to determine the intake air-flow.

The measured velocities were used to determine the intake air flow, and the obtained results are presented in TABLE 3.

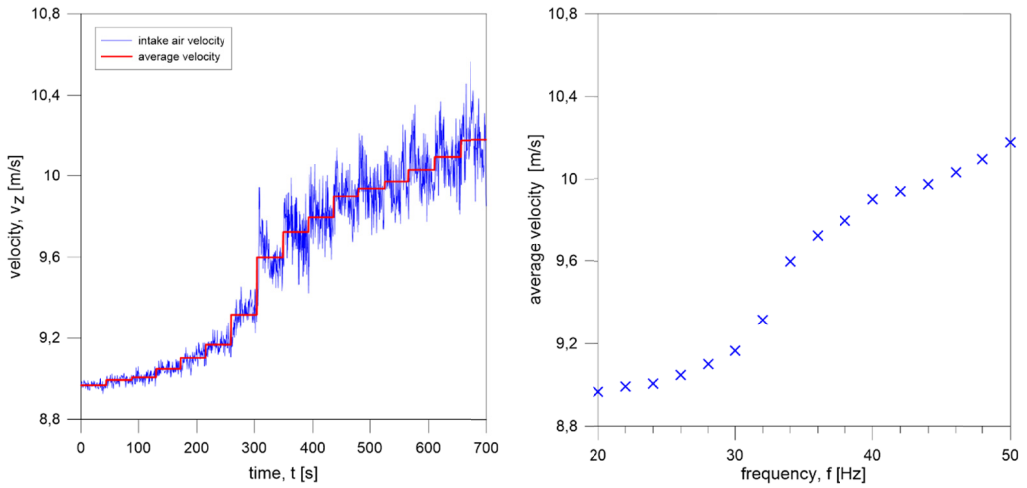


Fig. 3. Plot of the recorded intake air velocity vs. average speed

TABLE 3

Air-flow vs. inverter frequency

Frequency [Hz]	Average air velocity [m/s]	Intake air-flow [m ³ /s]	Frequency [Hz]	Average air velocity [m/s]	Intake air-flow [m ³ /s]
20	8.967	0.158	36	9.724	0.172
22	8.992	0.159	38	9.796	0.173
24	9.006	0.159	40	9.899	0.175
26	9.047	0.160	42	9.936	0.176
28	9.101	0.161	44	9.971	0.176
30	9.166	0.162	46	10.028	0.177
32	9.317	0.165	48	10.097	0.178
34	9.600	0.170	50	10.178	0.180

The obtained results indicate that the difference between the lowest and the highest value of the intake air is approximately 0.02 m³/s. Losses on the fan were neglected in the considerations, and the authors assumed that the intake airflow was equal to the flow entering the fluidisation column. The velocity of the gas entering the fluidisation column was determined during the next step, based on equation (7):

$$v_w = \frac{\dot{V}_z}{\pi \left(\frac{D}{2}\right)^2} \quad (7)$$

where:

- v_w – velocity of the air entering the fluidisation column, [m/s],
- D – diameter of the fluidisation column, [m].

The results for the calculated velocity in the empty section of the fluidisation column are presented in Table 4. Knowing the mass of the bed poured into the column ($m = 4.7$ kg), its skeleton density ($\rho_s = 2800$ kg/m³) and the poured height of the bed, the initial porosity of the bed was calculated according to equation (8):

$$\varepsilon_0 = \left(1 - \frac{4m}{\rho_s \cdot h \cdot \pi \cdot D^2} \right) \cdot 100\% \quad (8)$$

where:

$\varepsilon(f)$ – bed porosity, as a function of the frequency pre-set on the fan inverter, [%],

$h(f)$ – bed height, as a function of the frequency pre-set on the fan inverter, [m].

A video was recorded during the experiment in order to present the bed height for individual inverter frequencies. Fig. 4 presents photographs of the fluidisation column filled with the bed, including the indicated levels of bed layer deposits.

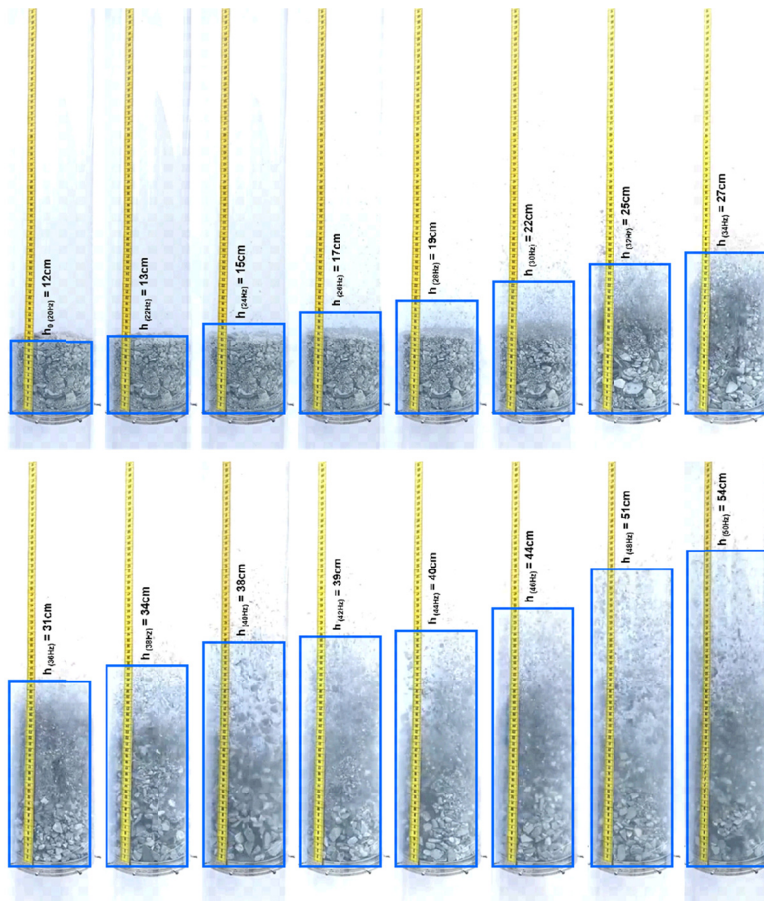


Fig. 4. Recorded bed heights vs. pre-set inverter frequency

The recorded height of the fluidal bed shall enable the determination of porosity for that bed at every stage of the experiment, depending on the pre-set frequency. TABLE 4 presents the results for bed porosity as a function of the pre-set inverter frequency.

TABLE 4

Gas velocity in the empty fluidisation column, bed height during the experiment and bed porosity vs. frequency

Frequency [Hz]	Velocity [m/s]	Deposit height [m]	Bed porosity [%]
20	7.881	0.12	30.43
22	7.903	0.13	35.78
24	7.915	0.15	44.34
26	7.952	0.17	50.89
28	7.999	0.19	56.06
30	8.056	0.22	62.05
32	8.189	0.25	66.61
34	8.437	0.27	69.08
36	8.546	0.31	73.07
38	8.609	0.34	75.45
40	8.700	0.38	78.03
42	8.733	0.39	78.59
44	8.764	0.40	79.13
46	8.814	0.44	81.03
48	8.874	0.51	83.63
50	8.946	0.54	84.54

The following graphs (Figs. 5, 6) present the relationship between the bed height and porosity versus the pre-set inverter frequency and the actual velocity inside the fluidisation column. Fig. 7 presents the relationship between bed porosity and its height inside the fluidisation column.

During an analysis of the bed height, it was observed that the bed height gradually increases with the increasing inverter frequency, followed by a momentary plateau on the graph, which may suggest the time at which the bed becomes completely loose and all its grain classes become mixed. The last stage presented in Fig. 5, above the frequency of 40 Hz, changes into a more steep line, indicating that the static bed becomes a fluidised bed. This is also the case in Fig. 6, which presents the fluidised bed porosity versus the inverter frequency and velocity. In the initial stage of the performed experiment, bed porosity initially increased until the inverter was set to approximately 40 Hz, after which the graph shows a distinct plateau, potentially indicating intense grain mixing throughout the entire bed.

Knowledge of the porosity of an individual, and recorded inverter frequency enables the determination of fluid velocity upon contact with the bed layer, hereinafter referred to as fluidisation velocity, expressed using equation (9):

$$v_f = \frac{\dot{V}_z}{\pi \frac{D^2}{4} \cdot \varepsilon(f)} \quad (9)$$

where: v_f – fluidisation velocity during the experiment, [m/s].

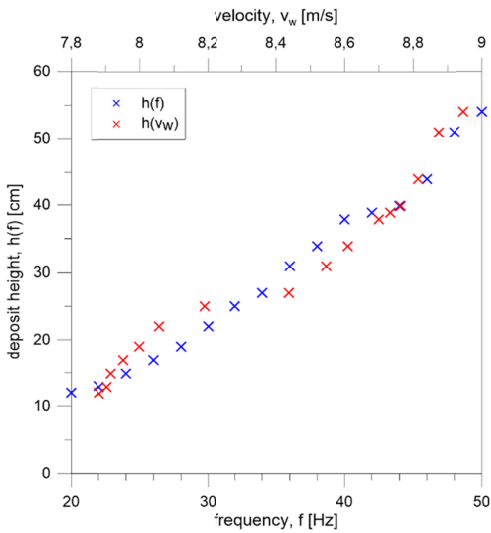


Fig. 5. Bed height vs. pre-set inverter frequency and vs. velocity inside the fluidisation column

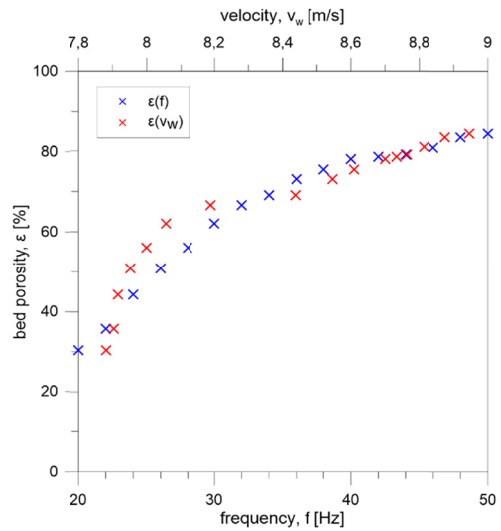


Fig. 6. Bed porosity vs. pre-set inverter frequency and vs. velocity inside the fluidisation column

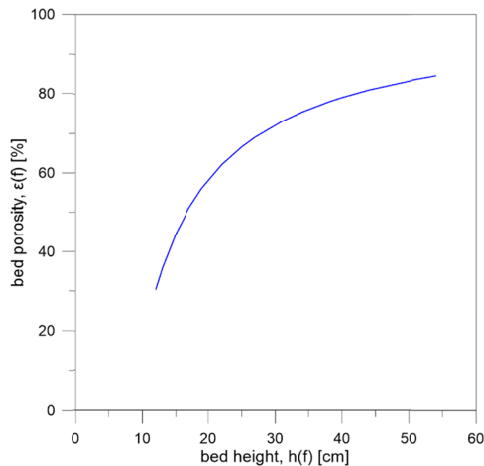


Fig. 7. Fluidised bed porosity vs. its height in the fluidisation column

The fluidisation theory states that gas pressure decreases with its increasing velocity, and the last element which has to be determined is the dynamic fluid pressure at the point of contact with the poured grain layer. This pressure was determined using equation (10):

$$p = \frac{\rho_G \cdot v_f^2}{2} \quad (10)$$

where: p – gas pressure exerted on the bed layer, [Pa].

TABLE 5 presents the obtained results, and Fig. 8 presents a graph of fluidisation velocity versus the pre-set inverter frequency and the inlet velocity inside an empty fluidisation column. Fig. 9 shows a dynamic gas pressure variability graph.

TABLE 5

Fluidisation velocity and dynamic pressure of the fluid

Frequency [Hz]	Fluidisation velocity [m/s]	Dynamic pressure [Pa]	Frequency [Hz]	Fluidisation velocity [m/s]	Dynamic pressure [Pa]
20	25.899	402.455	36	11.696	82.082
22	22.088	292.720	38	11.411	78.132
24	17.850	191.179	40	11.150	74.589
26	15.625	146.486	42	11.112	74.084
28	14.268	122.147	44	11.075	73.594
30	12.982	101.127	46	10.878	70.998
32	12.295	90.695	48	10.611	67.559
34	12.214	89.503	50	10.582	67.183

The presented results confirm the fluidisation assumption, where fluid pressure decreases with increasing fluid velocity. The initial dynamic gas pressure in the experiment was approximately 405 Pa. Up to the frequency of 30 Hz, an intensive pressure drop was observed, and dynamic pressure stabilises above 40 Hz, which is characteristic of a fluidised bed, according to Fig. 1.

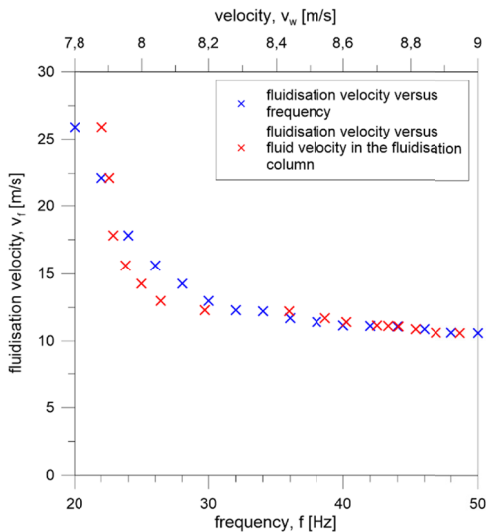


Fig. 8. Fluid velocity upon contact with the bed layer versus frequency and inlet velocity

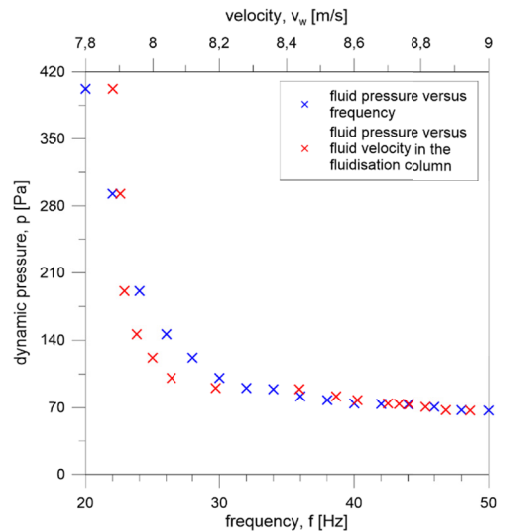


Fig. 9. Fluid velocity upon contact with the bed layer versus frequency and inlet velocity

4. Comparison of theoretical and experimental results

The performed theoretical considerations and experimental studies enabled verification of the concept related to the possibility of fluidic transport of rock material during outbursts of rocks and gases, bypassing sorption phenomena. The minimum fluidisation velocity for individual grain classes is mainly present in outbursts of dolomite and gas, as estimated in Chapter 2. The Archimedes number was also determined, and it indicated that the considered flow would be turbulent. This value was used to determine the hovering velocity for individual grains. This velocity was in the range of 18-45 m/s for the highest grain class.

The consumption of intake air during the experiment was recorded and used to calculate the intake airflow into the fluidisation column. The intake air velocity was in the range of 7.8-9.0 m/s, which means it was higher than the minimum fluidisation velocity.

Upon contact between the gas and the bottom layer of the bed, gas fills the free inter-grain spaces, where it increases its velocity proportionally to the constriction of free space, according to Bernoulli's law. The maximum velocity was just under 26 m/s. Gas pressing against the bottom layer of the bed at such velocity exerts dynamic pressure on the bed, resulting in the loosening of the bed.

During the first seconds of the experiment, corresponding to frequencies of 20-28 Hz and the outlet velocity at the fluidisation column of 7.8-8 m/s, the motion of only the smallest grain class of 1-2 mm was observed. Higher classes were only loosened despite the minimum fluidisation velocity being exceeded. This is presumably a result of the efficiency of the fan, which did not generate the equivalent of the intake airflow. Higher grain classes were also mixed according to the grain distribution of post-outburst masses, in which the 8-20 mm class was the largest fraction (TABLE 6), and the higher grain classes could cover smaller grains and block their flow together with the airflow. A gradual increase in the size of grains lifted in the column was observed for the subsequent inverter indications (30-38 Hz), however, these highest grain classes still form the immobile part of the bed. It was only from the frequency of 40 Hz, corresponding to the average intake velocity of 8.7 m/s and the fluidisation velocity of 11 m/s, that the highest grain class was mobilised. Fluidisation velocity stabilised at a level of 10.6 m/s during the final stage of the experiment. This value is higher than the minimum fluidisation velocity (max. 5.2 m/s) for each grain class and lower than the hovering velocity (min. 18 m/s), which means that the bed is in equilibrium with the fluid flowing around it and is not blown outside the fluidisation column.

TABLE 6

Percentage fractions of individual grain classes

Grain class [mm]	Percentage share [%]
20-50	29.73
8-20	30.88
4-8	21.55
2-4	11.75
1-2	6.08

5. Discussion

When undertaking the topic of rock and gas outburst in terms of the transport type, one should also verify whether the calculated, theoretical values of parameters such as the minimum fluidisation velocity or the hovering velocity, as well as the empirically determined values of fluidisation velocity can occur during a gas-geodynamic event under the conditions present in copper ore mines. A case study for the parameters of the rock-gas system recorded during a rock and gas outburst at the Rudna copper ore mine in Poland was performed for the purpose [4].

Assuming the parameters of the rock-gas system: porosity $\varepsilon = 20\%$ and gas pressure $p_g = 4$ MPa, the estimated volume of gas from 1 m^3 of the porous rock was 8 m^3 . According to the data [4], solid rock with a volume of approximately 250 m^3 was crushed during the outburst, which means that the amount of gas corresponding to this volume was approximately 2000 m^3 . The velocity of gas originating from the avalanche-type rock crushing in the direction of the heading was estimated according to equation (11):

$$v_p = \frac{V_G}{t_w \cdot S_w} \quad (11)$$

where:

- v_p – the bed flow rate, [m/s],
- V_G – the volume of gas emitted from rock pores, [m^3],
- t_w – the outburst duration, [s],
- S_w – the free cross-section of the heading, [m^2].

The free cross-section of the heading was based on Fig. 10, which is an actual sketch made at the outburst site. During the final stage of the outburst, the free cross-section of the heading was approximately 5% of the entire cross-section (18 m^2). A velocity analysis was also performed for a series of free cross-sections of the heading, at the levels of: 50%, 25% and approximately 10%.

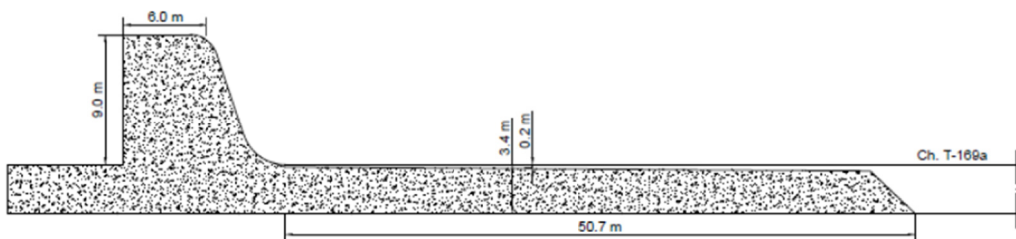


Fig. 10. Sketch of the heading after outburst at the O/ZG "Rudna" in 2009

The average outburst duration was approximately 1-2 minutes, according to the report of the miners at the mine, where the outburst of rocks and gas took place. Hence, the following values were accepted in the estimation of the bed flow rate: $t_w = 30 \text{ s}, 60 \text{ s}, 120 \text{ s}, 180 \text{ s}$. TABLE 7 presents the obtained results and the plot (Fig. 11) of bed flow rates related to the ranges of fluidisation velocity (minimum fluidisation velocity for the lowest grain class and hovering velocity for the highest grain class).

TABLE 7

Estimated bed flow rate during the rock and gas outburst

Outburst duration [s]	Free cross-section of the heading [m ²]	Bed flow velocity [m/s]
30	18 (100%)	3.70
	9 (50%)	7.41
	4.5 (25%)	14.81
	2 (~10%)	33.33
	1 (~5%)	66.67
60	18	1.85
	9	3.70
	4.5	7.41
	2	16.67
	1	33.33
120	18	0.93
	9	1.85
	4.5	3.70
	2	8.33
	1	16.67
180	18	0.62
	9	1.23
	4.5	2.47
	2	5.56
	1	11.11

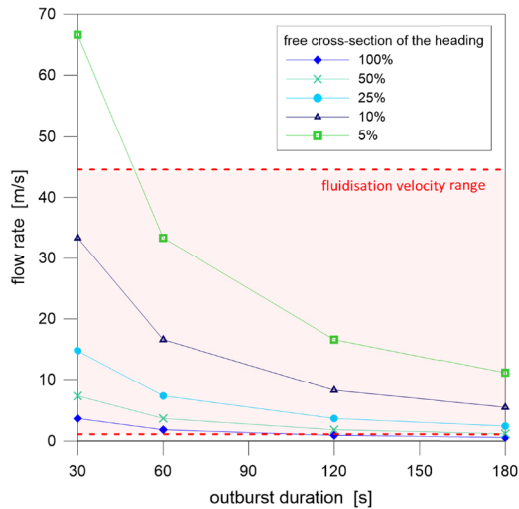


Fig. 11. Range of fluidisation velocities related to bed velocity at different cross-sections of the heading

Analysis of the obtained results leads to a conclusion that if the heading is not filled with rock material (100% free cross-section), fluidisation is possible if the outburst lasts no longer than 60 seconds. If this duration is exceeded, the velocity of grains in lower grain classes will be too low. In the case of a free cross-section corresponding to 50%, 25% and 10% of the full cross-section of the heading, the outburst duration for which fluidisation is possible may be in the range of 30-180 seconds. If the cross-section of the heading is only 5% free, as was the case during the final stage of the outburst at the “Rudna” mine in Poland (Fig. 10), fluidisation will be possible if the duration of bed transport exceeds approximately 60 seconds. In the case of shorter durations of rock and gas outburst, the velocity of the lowest grain class will exceed the hovering velocity, and thus the transport becomes pneumatic.

6. Conclusion

This paper presents considerations on the fluidisation of rock material during the outburst of rocks and gases. Chapter One describes the topic of gas-geodynamic phenomena in mining. Gas accumulated in the porous structure is responsible for an outburst of rocks and gases at coal and copper ore mines. Both coal and dolomite are crushed as a result of sudden decompression of free gas, not bound by sorption. In the case of coal, the transport is fluid in nature, and intense desorption is responsible for it, while desorption is low or absent in dolomite. The analyses carried out in the paper were intended to verify whether fluidisation-based transport is still possible despite the lack of sorption processes.

Determination of the theoretical values of the minimum fluidisation velocity, the Archimedes number and the hovering velocity, and their summary with parameters obtained during the experiment, such as intake velocity at the fluidisation column, fluidisation velocity or dynamic pressure allowed the conclusion that fluidisation of rock material is possible if rock material is uniformly crushed during rock and gas outburst and if constant gas flow at a velocity not exceeding 45 m/s is guaranteed. An analysis of the phenomenon of rock and gas outburst in copper ore mines confirmed that the flow of gas released from the porous volume of the rock may reach velocities required to sustain fluidisation.

References

- [1] A. Koterak, J. Kabiesz, R. Patyńska, Natural hazards in underground coal mining in Poland against the background of the selected European countries of the world. *Przegląd Górniczy* **1**, 15-30 (2015).
- [2] J. Feng, E. Wang, H. Ding, Q. Huang, X. Chen, Deterministic seismic hazard assessment of coal fractures in underground coal mine: A case study. *Soil Dynamics and Earthquake Engineering* **129**, 105921 (2020). DOI: <https://doi.org/10.1016/j.soildyn.2019.105921>
- [3] P. Małkowski, Z. Niedbalski, A comprehensive geomechanical method for the assessment of rockburst hazards in underground mining. *International Journal of Mining Science and Technology* **30** (3), 345-355, (2020). DOI: <https://doi.org/10.1016/j.ijmst.2020.04.009>
- [4] K. Kozieł, N. Skoczylas, K. Soroko, S. Gola, Gas and Dolomite Outbursts in Ore Mines – Analysis of the Phenomenon and the Energy Balance. *Energies* **13**, 2999 (2020). DOI: <https://doi.org/10.3390/en13112999>
- [5] A. Gonet, S.A. Stryczek, Innovative Technology of Tight Liquidation of Workings on the Example of the Wieliczka Salt Mine. *Archives of Mining Sciences* **66** (1), 3-12 (2021). DOI: <https://doi.org/10.24425/ams.2021.136688>

- [6] T. Janoszek, J. Krawczyk, Methodology Development and Initial Results of CFD Simulations of Methane Distribution in the Working of a Longwall Ventilated in a Short “Y” Manner. *Archives of Mining Sciences* **67** (1), 3-24 (2022). DOI: <https://doi.org/10.24425/ams.2022.140699>
- [7] R. Lama, J. Bodziony, Management of outburst in underground coal mines. *International Journal of Coal Geology* **35** (1-4), 83-115 (1998). DOI: [https://doi.org/10.1016/S0166-5162\(97\)00037-2](https://doi.org/10.1016/S0166-5162(97)00037-2)
- [8] J. Topolnicki, M. Wierzbicki, N. Skoczylas, Wyrzuty skalno-gazowe w świetle badań laboratoryjnych i pomiarów kopalnianych. *Archives of Mining Sciences* **49**, 99-116 (2004).
- [9] A. Kidybiński, The effect of porosity and the strength of coal on the dynamics of coal and methane outburst – The bpm modeling. *Archives of Mining Sciences* **56**, 415-426 (2011).
- [10] N. Skoczylas, Laboratory study of the phenomenon of methane and coal outburst. *International Journal of Rock Mechanics and Mining Sciences* **55**, 102-107 (2012). DOI: <https://doi.org/10.1016/j.ijrmmms.2012.07.005>
- [11] N. Skoczylas, Estimating gas and rock outburst risk on the basis of knowledge and experience – the expert system based on fuzzy logic. *Archives of Mining Sciences* **59** (1), 41-52 (2014). DOI: <https://doi.org/10.2478/amsc-2014-0003>
- [12] X. Pan, H. Cheng, J. Chen, X. Zhou, An experimental study of the mechanism of coal and gas outbursts in the tectonic regions. *Engineering Geology* **279**, 105883 (2020). DOI: <https://doi.org/10.1016/j.enggeo.2020.105883>
- [13] L. Wang, Z. Lu, D. Chen, Q. Liu, P. Chu, L. Shu, B. Ullah, Z. Wen, Safe strategy for coal and gas outburst prevention in deep-and-thick coal seams using a soft rock protective layer mining. *Safety Science* **129**, 104800 (2020). DOI: <https://doi.org/10.1016/j.ssci.2020.104800>
- [14] M. Gawor, S. Wasilewski, Investigations of dynamic properties of an integrated methane and rock outburst sensor. *Measurement* **186**, 110178 (2021). DOI: <https://doi.org/10.1016/j.measurement.2021.110178>
- [15] W. Wang, H. Wang, B. Zhang, S. Wang, W. Xing, Coal and gas outburst prediction model based on extension theory and its application. *Process Safety and Environmental Protection* **154**, 329-337 (2021). DOI: <https://doi.org/10.1016/j.psep.2021.08.023>
- [16] L. Shu, K. Wang, Z. Liu, W. Zhao, N. Zhu, Y. Lei, A novel physical model of coal and gas outbursts mechanism: Insights into the process and initiation criterion of outbursts. *Fuel* **323**, 124305 (2022). DOI: <https://doi.org/10.1016/j.fuel.2022.124305>
- [17] G. Zhang, E. Wang, Ch. Zhang, Z. Li, D. Wang, A comprehensive risk assessment method for coal and gas outburst in underground coal mines based on variable weight theory and uncertainty analysis. *Process Safety and Environmental Protection* **167**, 97-111 (2022). DOI: <https://doi.org/10.1016/j.psep.2022.08.065>
- [18] K. Kozieł, A. Nowakowski, L. Sitek, N. Skoczylas, Rock and Gas Outbursts in Copper Mines: Use of Brazilian Tests to Evaluate the Work of Disintegration of Rock Resulting from Stresses Produced by Gas Present in its Porous Structure. *Rock Mechanics and Rock Engineering* **55**, 6209-6225 (2022). DOI: <https://doi.org/10.1007/s00603-022-02955-z>
- [19] Ch. Fan, S. Li, M. Luo, W. Du, Z. Yang, Coal and gas outburst dynamic system. *International Journal of Mining Science and Technology* **27** (1), 49-55 (2017). DOI: <https://doi.org/10.1016/j.ijmst.2016.11.003>
- [20] D.J. Black, Review of coal and gas outburst in Australian underground coal mines. *International Journal of Mining Science and Technology* **29** (6), 815-824 (2019). DOI: <https://doi.org/10.1016/j.ijmst.2019.01.007>
- [21] E.Y. Wang, P. Chen, Z.T. Liu, Y.J. Liu, Z.H. Li, X.L. Li, Fine detection technology of gas outburst area based on direct current method in Zhuxianzhuang Coal Mine, China. *Safety Science* **115**, 12-18 (2019). DOI: <https://doi.org/10.1016/j.ssci.2019.01.018>
- [22] Ch. Zhang, E. Wang, J. Xu, S. Peng, A new method for coal and gas outburst prediction and prevention based on the fragmentation of ejected coal. *Fuel* **287**, 119493 (2021). DOI: <https://doi.org/10.1016/j.fuel.2020.119493>
- [23] J. Drzymala, P.B. Kowalczyk, M. Oteng-Peprah, D. Foszcz, A. Muszer, T. Henc, A. Luszczkiewicz, Application of the grade-recovery curve in the batch flotation of Polish copper ore. *Minerals Engineering* **49**, 17-23 (2013). DOI: <https://doi.org/10.1016/j.mineng.2013.04.024>
- [24] W. Kaczmarek, M. Twardowski, M. Wasilewska-Błaszczyk, Practical aspects of lithological types modelling in cu-ag ore Igom deposit (legnica-głogów copper district). *Biuletyn Państwowego Instytutu Geologicznego* **468**, 209-226 (2017). DOI: <https://doi.org/10.5604/01.3001.0010.0113>

- [25] A. Pajdak, K. Godyń, M. Kudasik, T. Murzyn, The use of selected research methods to describe the pore space of dolomite from copper ore mine, Poland. *Environmental Earth Sciences* **76**, 389 (2017). DOI: <https://doi.org/10.1007/s12665-017-6724-4>
- [26] W. Kaczmarek, M. Wasilewska-Błaszczuk, M. Dudek, The impact of lithological variability of reservoir rocks on the quality parameters of the Cu-Ag deposit, Lubin-Głogów Copper District (LGCD). *Biuletyn Państwowego Instytutu Geologicznego* **472**, 105-120 (2018). DOI: <https://doi.org/10.5604/01.3001.0012.6919>
- [27] S. Speczik, K. Zieliński, T. Bieńko, A. Pietrzela: The prospecting strategy for a deep Cu-Ag ore deposit in Poland – An anatomy of success. *Ore Geology Reviews* **131**, 104053 (2021). DOI: <https://doi.org/10.1016/j.oregeorev.2021.104053>
- [28] A. Mirek, M. Laskowski, A. Respondek, A. Hryciuk, Wyrzut gazów i skał z O/ZG „Rudna” – incydent czy tendencja? *Prace Nauk. GIG: Górnictwo i Środowisko* **4/3**, 275-288 (2010).
- [29] M. Wierzbicki, M. Młynarczuk, Structural aspects of gas and dolomite outburst in Rudna copper mine, Poland. *International Journal of Rock Mechanics and Mining Sciences* **57**, 113-118 (2013). DOI: <https://doi.org/10.1016/j.ijrmm.2012.08.007>
- [30] M. Biliński, A. Hryciuk, M. Laskowski, A. Mirek, Zagrożenie wyrzutami w KGHM „Polska Miedź” S.A. O/ZG „Rudna” – stan po czterech latach od wyrzutu. *Bezpieczeństwo Pracy i Ochrona Środowiska w Górnictwie* **1**, 24-28 (2015).
- [31] K. Król, G. Dzik, Zagrożenie gazogeodynamiczne i sposoby jego zwalczania w kopalniach rud miedzi w świetle prac zespołu doradczo-opiniodawczego ds. analizy zjawisk gazogeodynamicznych w KGHM Polska Miedź S.A. *Bezpieczeństwo Pracy i Ochrona Środowiska w Górnictwie* **5**, 2-9 (2020).
- [32] B. Beamish, P.J. Crosdale, Instantaneous outbursts in underground coal mines: An overview and association with coal type. *International Journal of Coal Geology* **35**, 27-55 (1998). DOI: [https://doi.org/10.1016/S0166-5162\(97\)00036-0](https://doi.org/10.1016/S0166-5162(97)00036-0)
- [33] Y. Cao, G.D. Mitchell, A. Davis, D. Wang, Deformation metamorphism of bituminous and anthracite coals from China. *International Journal of Coal Geology* **43** (1-4), 227-242 (2000). DOI: [https://doi.org/10.1016/S0166-5162\(99\)00061-0](https://doi.org/10.1016/S0166-5162(99)00061-0)
- [34] S. Li, T. Zhang, Catastrophic mechanism of coal and gas outbursts and their prevention and control. *Mining Science and Technology (China)* **20** (2), 209-214 (2010). DOI: [https://doi.org/10.1016/S1674-5264\(09\)60186-1](https://doi.org/10.1016/S1674-5264(09)60186-1)
- [35] M. Kudasik, N. Skoczylas, Analyzer for measuring gas contained in the pore space in rocks. *Measurement Science and Technology* **28** (10), 105901 (2017). DOI: <https://doi.org/10.1088/1361-6501/aa812d>
- [36] K. Kozieł, J. Topolnicki, N. Skoczylas, The Intensity of Heat Exchange between Rock and Flowing Gas in Terms of Gas-Geodynamic Phenomena. *Entropy* **23**, 556 (2021). DOI: <https://doi.org/10.3390/e23050556>
- [37] J. Topolnicki, M. Wierzbicki, Transport sedimentacyjny mas powyrzutowych. *Prace Instytutu Mechaniki Górniczej PAN* **18** (3), 67-73 (2016)
- [38] K. Kozieł, J. Janus, Force Exerted by Gas on Material Ejected During Gas-geodynamic phenomena. Analysis and Experimental Verification of Theory. *Archives of Mining Sciences* **67** (3), 491-508 (2022). DOI: <https://doi.org/10.24425/ams.2022.142412>
- [39] J. Topolnicki, M. Wierzbicki, N. Skoczylas, J. Sobczyk, Badania kinetyki uwalniania metanu z próbek węglowych pochodzących z wybranych miejsc w pokładzie 409/3 kopalni „Zofiówka”. *Prace Instytutu Mechaniki Górniczej PAN* **7** (3-4), 203-214 (2005).
- [40] S. Wang, D. Elsworth, J. Liu, Rapid decompression and desorption induced energetic failure in coal. *Journal of Rock Mechanics and Geotechnical Engineering* **7**, 345-350 (2015). DOI: <http://dx.doi.org/10.1016/j.jrmge.2015.01.004>
- [41] W. Zhao, Y.P. Cheng, H.N. Jiang, K. Jin, H.F. Wang, L. Wang, Role of the rapid gas desorption of coal powders in the development stage of outbursts. *Journal of Natural Gas Science and Engineering* **28**, 491-501 (2016). DOI: <https://doi.org/10.1016/j.jngse.2015.12.025>
- [42] L.H. Xu, C.L. Jiang, Initial desorption characterization of methane and carbon dioxide in coal and its influence on coal and gas outburst risk. *Fuel* **203**, 700-706 (2017). DOI: <https://doi.org/10.1016/j.fuel.2017.05.001>
- [43] D.D. Yang, Y.J. Chen J., Tang, X.W. Li, C.L. Jiang, C.J. Wang, C.J. Zhang, Experimental research into the relationship between initial gas release and coal-gas outbursts. *Journal of Natural Gas Science and Engineering* **50**, 157-165 (2018). DOI: <https://doi.org/10.1016/j.jngse.2017.12.015>

- [44] B. Zhou, J. Xu, F. Yan, S. Peng, Y. Gao, Q. Li, L. Cheng, Effects of gas pressure on dynamic response of two-phase flow for coal-gas outburst. *Powder Technology* **377**, 55-69 (2021).
DOI: <https://doi.org/10.1016/j.powtec.2020.08.065>
- [45] S.K. Gupta, V.K. Agarwal, S.N. Singh, V. Seshardi, D. Mills, J. Singh, Ch. Prakash, Prediction of minimum fluidization velocity for fine tailings materials. *Powder Technology* **196** (3), 263-271 (2009).
DOI: <https://doi.org/10.1016/j.powtec.2009.08.003>
- [46] Z. Orzechowski, J. Prywer, R. Zarzycki, *Mechanika płynów w inżynierii środowiska*. Wydawnictwo Naukowe PWN, ISBN/ISSN: 9788301198480 (2018).